MEASUREMENT PROCESS AND INVERSIONS USING HELIOSEISMIC NORMAL-MODE COUPLING

Shravan Hanasoge[*]

ABSTRACT

Normal modes are coupled by the presence of perturbations in the Sun, providing a unique and little-explored helioseismic technique with which to image the solar interior. The process of measuring coupling between normal modes is straightforward, much more so when compared with other prevalent helioseismic techniques. The theoretical framework to interpret these measurements is well developed with the caveat that it applies only in the case where the entire surface of the Sun is observed. In practice however, the limited visibility of the Sun and line-of-sight related effects diminish the resolution of the technique. Here, we compute realistic sensitivities of normal-mode coupling measurements to flows in the solar interior and describe how to mitigate the sometimes overwhelming effect of leakage. The importance of being able to isolate individual spherical harmonics and observe the full Sun, to which future solar observatories may aspire, is thus highlighted in our results. In the latter part of the article, we describe the noise model for the variance of coupling coefficients, a critical component to the process of inference.

Keywords: Sun: helioseismology—Sun: interior—Sun: oscillations—waves—hydrodynamics

hanasoge@tifr.res.in

[*] Department of Astronomy & Astrophysics, Tata Institute of Fundamental Research, Mumbai 400005, India
Center for Space Science, New York University Abu Dhabi, UAE

1. INTRODUCTION

Global-mode helioseismology has led to robust inferences of axisymmetric properties of the Sun such as its structure (as a function of radius) and rotation (with radius and latitude; e.g. Christensen-Dalsgaard 2002). However global-mode frequencies possess very little sensitivity to meridional circulation and non-axisymmetric features such as convection. Nevertheless, frequency series of mode harmonics, i.e. $\phi_{\ell m}(\omega)$, where ω is temporal frequency, ℓ is spherical harmonic degree, m the azimuthal order and ϕ the observed line-of-sight projected surface velocity, contain significant information that has not been fully exploited. In global-mode analyses, the auto-correlation quantity $\phi_{\ell m}^* \phi_{\ell m}$ is the primary measurement. Whereas, the more general quantity $\phi_{\ell' m'}(\omega') \phi_{\ell m}^*(\omega)$, which is the wavefield correlation in Fourier domain, contains phase information (unlike global-mode frequencies), providing insight into non-axisymmetric and time-varying features in the solar interior. There have been attempts to infer meridional circulation and convection using these measurements (e.g. Schad et al. 2011; Woodard et al. 2013; Woodard 2014, 2016) but the technique still needs to be refined and understood better in order to place faith in subsequent inferences. Based on the original work by Lavely & Ritzwoller (1992) and techniques of terrestrial seismology (Dahlen & Tromp 1998), Hanasoge et al. (2017) and Hanasoge (2017) computed kernels for flows and magnetic fields respectively (also see Cutler 2017). However, these kernels were predicated on being able to observe the solar surface in its entirety and thus do not capture systematical errors associated with realistic observations of the Sun.

The premise of normal-mode coupling is as follows. Consider the eigenfunctions to a reference model of the Sun, i.e. a structure model that is non-rotating, non-convecting, non-magnetic and radially stratified (e.g. model S, Christensen-Dalsgaard et al. 1996). These eigenfunctions are orthogonal and form a complete basis (Christensen–Dalsgaard 2003). Assuming the eigenfunctions of the real Sun to be slightly perturbed forms of the reference eigenfunctions, we may express the former as linear combinations of the latter. Thus the eigenfunction of a given mode in the real Sun is actually a mixture of eigenfunctions of the reference Sun, and the modes of the real Sun are said to be 'coupled' with respect to the reference. However since we only observe the surface, it is not possible to measure the eigenfunction, a 3-D quantity, in the Sun. We thus use the measurement $\phi_{\ell' m'}(\omega') \phi_{\ell m}^*(\omega)$ as a proxy for the extent of coupling. Because we only observe half the Sun, and in practice a third, owing to limb-darkening effects, it is not possible to isolate modes in terms of spherical harmonics. Thus, even in the reference model, the quantity $\phi_{\ell' m'}(\omega') \phi_{\ell m}^*(\omega)$ is non-zero owing to effects such as leakage, realization noise (waves in the Sun are stochastically excited), and other systematic effects. Mode coupling induced by systematical effects must therefore be computed with great care since they contribute a dominant fraction of measured mode correlations (for an equivalent approach in time-distance helioseismology, see e.g. Gizon & Birch 2004).

The uncertainty principle indicates that windowing in the spatial domain results in a broadening in the spherical-harmonic domain, causing mode signal to "leak" from one spherical harmonic to neighbouring channels. To characterize this effect, Schou & Brown (1994) introduced the so-called leakage matrix $L_{\ell' m'}^{\ell m}$, where (ℓ, m) and (ℓ', m') are two modes. Leakage between modes diminishes rapidly with increasing $|\ell - \ell'|$ and $|m - m'|$. One consequence of leakage is that the wavefield correlation $\phi_{\ell' m'}^*(\omega') \phi_{\ell m}(\omega)$ actually measures the coupling between a number of modes, the details of which depend in complicated ways on the resonant frequencies of the modes and specific wavenumbers in question. Mode leakage in turn has the effect of garbling the sensitivity of the measurement to underlying perturbations. In other words, the inability to isolate a specific

modal harmonic in the observations translates to inferences of the perturbation, i.e. it is impossible to retrieve individual wavenumbers. The important issues are therefore of quantifying, accounting for and mitigating this effect.

The measured signal at any given point in the frequency-wavenumber spectrum comprises contributions from modes at all temporal frequencies (i.e. all radial orders) at that specific spatial frequency. This is due to the fact that we cannot observe the internal layers of the Sun and isolate specific radial orders. However, what makes it feasible to identify (approximately, at any rate) individual radial orders is that mode power, which is well approximated as a Lorentzian, falls rapidly, away from resonance. Thus close to resonance (within a couple of mode linewidths), the observed signal is dominated by the mode at that radial order, and we therefore associate signal within that region of the spectrum with that radial order. Because space-based instruments contain essentially no temporal gaps, the observations can be well isolated in temporal frequency. Using this reasoning, we use temporal frequency as a means to discern radial order, and stay within a couple of linewidths of resonance.

The helioseismic wave equation (e.g. Christensen-Dalsgaard 2002; Gizon et al. 2010) is linear and as a consequence, the wavefield at different temporal frequency channels may be treated independently. However, convection comprises non-axisymmetric time-varying features, introducing a convolution in the frequency domain and thereby mixing frequency channels. The analysis discussed in e.g. Woodard (2016) and Hanasoge et al. (2017) address this issue by considering mode-correlation measurements at different frequencies across a mode. As discussed earlier though, these measurements need to made very close to resonance. One consequence therefore of limiting the frequency interval of study (to avoid straying too far from resonance) is that it is not possible to study convective features at short lifetimes (the shorter the lifetime, the larger the associated frequency).

In this article, we incorporate the systematical issues associated with leakage and derive corresponding sensitivity functions for flows. We also construct a theoretical model for noise levels that are expected in these measurements.

2. THE FULLY VISIBLE SUN

The theory describing the connection between wavefield correlations and perturbations is detailed in Woodard (2016) and Hanasoge et al. (2017). To summarize the development, the sensitivity of coupled modes (ℓ, m, n) and (ℓ', m', n) due to flows in the interior is given by

$$\phi_{\ell'm'}^{\omega+\sigma} \phi_{\ell m}^{\omega*} = -2\omega(N_{\ell'} R_{\ell m}^{\omega*} |R_{\ell'm'}^{\omega+\sigma}|^2 + N_\ell R_{\ell'm'}^{\omega+\sigma} |R_{\ell m}^\omega|^2) \sum_{s,t} \int_\odot dr \, [iu_{st}(r,\sigma) K_{st}^u(r) + w_{st}(r,\sigma) K_{st}^w(r)],$$

(1)

where the dependence on temporal frequency ω is written now as a superscript, i.e. $\phi_{\ell m}^\omega = \phi_{\ell m}(\omega)$, σ is the inverse timescale associated with the flow, r is radius, $u_{st}(r,\sigma)$ denotes mass-conserving poloidal flow (see Eqs. 61 and 62 of Hanasoge et al. 2017) at harmonic degree s and azimuthal order t and $w_{st}(r,\sigma)$ the toroidal flow component (mass conserving by construction). The mode frequency and amplitude details are stored in terms N_ℓ and $R_{\ell m}^\omega$, the mode-normalization constant and Lorentzian respectively, where

$$R_{\ell m}^\omega = \frac{1}{(\omega_{n\ell m} - i\Gamma_{n\ell}/2)^2 - \omega^2} \approx \frac{1}{2\omega_{n\ell m}} \frac{1}{\omega_{n\ell m} - i\Gamma_{n\ell}/2 - \omega},$$

(2)

and $\Gamma_{n\ell}$ is the damping rate. The sensitivity kernels K_{st}^u and K_{st}^w are actually dependent on ℓ, m and ℓ', m' but to reduce notational burden, we do not explicitly state them. These kernels may be simplified significantly using asymptotic expressions derived in Woodard (2014) and Appendix A

$$K_{st}^u \approx \gamma_{tm}^{\ell' s\ell} \, g_{\ell'-\ell,s} \, \mathcal{K}_{n\ell}(r), \tag{3}$$

$$K_{st}^w \approx \gamma_{tm}^{\ell' s\ell} \, f_{\ell'-\ell,s} \, \mathcal{K}_{n\ell}(r), \tag{4}$$

where we slightly tweak the notation introduced by Woodard (2014) for the symbol γ, which is defined thus

$$\gamma_{tm}^{\ell' s\ell} = (-1)^{m+t} \sqrt{2s+1} \begin{pmatrix} \ell' & s & \ell \\ -(m+t) & t & m \end{pmatrix}. \tag{5}$$

The term in the parenthesis of equation (5), the Clebsch-Gordan coefficient, is non-zero only if the second row sums to zero (and hence there are only two independent parameters in the second row) and $|m+t| \le \ell', |t| \le s, |m| \le \ell, |\ell'-\ell| \le s, |\ell-s| \le \ell'$ and $|\ell'-s| \le \ell$. The symbols f and g are given by

$$f_{\ell'-\ell,s} = (-1)^{(s+\ell'-\ell-1)/2} \frac{(s-\ell'+\ell)!! \, (s+\ell'-\ell)!!}{\sqrt{(s-\ell'+\ell)! \, (s+\ell'-\ell)!}} \quad \text{(for odd } s+\ell'-\ell), \tag{6}$$

$$g_{\ell'-\ell,s} = i \, (-1)^{(s+\ell'-\ell)/2} \, (\ell'-\ell) \frac{(s-\ell'+\ell-1)!! \, (s+\ell'-\ell-1)!!}{\sqrt{(s-\ell'+\ell)! \, (s+\ell'-\ell)!}} \quad \text{(for even } s+\ell'-\ell), \tag{7}$$

where we emphasise that g now absorbs the factor of i from equation (1) and is therefore complex. The term $f_{\ell'-\ell,s}$ in equation (6) is defined to be non-zero only for odd $s+\ell'-\ell$ whereas $g_{\ell'-\ell,s}$ (Eq. [7]) is defined to be non-zero only for even $s+\ell'-\ell$ and $\ell' \ne \ell$. Finally the term $\mathcal{K}_{n\ell}(r)$ is given by

$$\mathcal{K}_{n\ell}(r) = \frac{(-1)^\ell}{\sqrt{2\pi}} \ell^{\frac{3}{2}} \rho r [U_{n\ell}^2 + \ell(\ell+1)V_{n\ell}^2], \tag{8}$$

where $U_{n\ell}(r)$ and $V_{n\ell}(r)$ are the radial and horizontal eigenfunctions for the (n,ℓ) mode (e.g., see Christensen–Dalsgaard 2003) and ρ is density.

We now consider measurements of mode coupling where $\ell = \ell'$ and s is odd (as studied, e.g. by Woodard 2016). The relationship between measurement and flow is given by

$$\phi_{\ell m+t}^{\omega+\sigma} \phi_{\ell m}^{\omega*} = H_{\ell\ell mt}^\sigma(\omega) \sum_{s,t} \gamma_{tm}^{\ell s\ell} \int_\odot dr \, [g_{0,s} \, u_{st}(r,\sigma) \, \mathcal{K}_{n\ell}^u(r) + f_{0,s} \, w_{st}(r,\sigma) \, \mathcal{K}_{n\ell}(r)]. \tag{9}$$

From equation (1), we denote the term that captures the mode power as a function of frequency through another symbol, H,

$$H_{\ell'\ell mt}^\sigma(\omega) = -2\omega(N_{\ell'} \, R_{\ell m}^{\omega*} \, |R_{\ell'm+t}^{\omega+\sigma}|^2 + N_\ell \, R_{\ell'm+t}^{\omega+\sigma} \, |R_{\ell m}^\omega|^2), \tag{10}$$

facilitating future analyses. From equation (7), we see that $g_{0,s} = 0$ and therefore the sensitivity of the measurement is given by

$$\phi_{\ell m+t}^{\omega+\sigma} \phi_{\ell m}^{\omega*} = H_{\ell\ell mt}^\sigma(\omega) \sum_{s,t} f_{0,s} \, \gamma_{tm}^{\ell s\ell} \int_\odot dr \, w_{st}(r,\sigma) \, \mathcal{K}_{n\ell}(r), \tag{11}$$

which is an elegant and simple expression. To aid analysis of observed data, Woodard (2016) introduce b-coefficients that are defined through the following reciprocal relationships,

$$\phi_{\ell m+t}^{\omega+\sigma} \phi_{\ell m}^{\omega*} = \sum_{s,t} \gamma_{tm}^{\ell s\ell} H_{\ell\ell mt}^{\sigma}(\omega) b_{st}^{\sigma}(n,\ell), \tag{12}$$

and the linear-least-squares approximation to the b coefficient is given by (adopted, for instance, by Woodard 2016),

$$b_{st}^{\sigma}(n,\ell) = \frac{\sum_{m,\omega} H_{\ell\ell mt}^{\sigma*} \gamma_{tm}^{\ell s\ell} \phi_{\ell m+t}^{\omega+\sigma} \phi_{\ell m}^{\omega*}}{\sum_{m,\omega} |H_{\ell\ell mt}^{\sigma} \gamma_{tm}^{\ell s\ell}|^2}, \tag{13}$$

where, in order to ensure that the wavefield is sampled closed to resonance, the frequency interval over which the sum is carried out must satisfy the criterion

$$\omega \in (\omega_{n\ell m} - \Gamma_{nl}, \omega_{n\ell m} + \Gamma_{nl}) \quad or \quad \omega \in (\omega_{n\ell m+t} - \Gamma_{nl} - \sigma, \omega_{n\ell m+t} + \Gamma_{nl} - \sigma). \tag{14}$$

Note that $\omega > 0$ in both these intervals. With this definition of the b coefficient, we have

$$g_{0,s} \int_{\odot} dr\, u_{st}(r,\sigma)\, \mathcal{K}_{\ell n}(r) + f_{0,s} \int_{\odot} dr\, w_{st}(r,\sigma)\, \mathcal{K}_{\ell n}(r) = b_{st}^{\sigma}(\ell,n), \tag{15}$$

with the poloidal term $u_{st}(r,\sigma)$ written only for the sake of completeness (Eq. [7] gives us $g_{0,s} = 0$). The flow system w_{st} is non-axisymmetric, representing a temporally and spatially fluctuating quantity. In order to stabilise the process of inference, we consider the power spectrum of w, i.e. the structure function of turbulence, which is axisymmetric and therefore a more stable quantity. As an aside, we note that because the flow field is real in the spatio-temporal domain, b coefficients need to obey certain parities, described in appendix C, which we explicitly enforce when computing them from the observations.

2.1. Inversion using wavefield correlations

We combine the measurements b_{st} over various ℓ and n so that the corresponding sum of kernels is focused around a localized region in radius. This gives

$$\int_{\odot} dr\, w_{st}(r,\sigma)\, f_{0,s} \sum_{\ell,n} \alpha^{\ell n}\, \mathcal{K}_{\ell n}(r) = \sum_{\ell,n} \alpha^{\ell n}\, b_{st}^{\sigma}(\ell,n), \tag{16}$$

$$\int_{\odot} dr\, w_{st}(r,\sigma)\, \mathcal{F}_s(r) = \beta_{st}^{\sigma}, \tag{17}$$

where $\mathcal{F}_s(r)$ is a radially focused function (such as a Gaussian centered around a given radius) and β_{st}^{σ} is the combined sum over b coefficients measured at various (n,ℓ), weighted by α. Now we multiply both sides by the complex conjugate of β and sum over t to obtain

$$\int_{\odot} dr\, dr' \sum_t w_{st}(r,\sigma)\, w_{st}^*(r',\sigma)\, \mathcal{F}_s(r)\, \mathcal{F}_s(r') = \sum_t |\beta_{st}^{\sigma}|^2. \tag{18}$$

If $\mathcal{F}_s(r)$ is generally well focused around some radius r_0, we may approximate $\mathcal{F}_s(r)\, \mathcal{F}_s(r') \approx \delta(r - r_0)\, \delta(r - r')$,

$$\int_{\odot} dr \sum_t |w_{st}(r,\sigma)|^2\, \delta(r - r_0) = \sum_t |\beta_{st}^{\sigma}|^2. \tag{19}$$

and we obtain

$$\sum_t |w_{st}(r_0, \sigma)|^2 = \mathcal{P}_s(r_0) = \sum_t |\beta_{st}^\sigma|^2. \tag{20}$$

Note that we have not stated considerations such as the tradeoff between sharpness of localisation in depth and the noise level (e.g. Pijpers & Thompson 1994) but these need also to be taken into account when deriving the weighted sum β_{st}^σ. Thus in the scenario where we are able to isolate individual modes in the spherical harmonic domain, we can obtain accurate estimates of convective properties in the interior. In the next section, we consider the realistic situation, where leakage and other effects play an important role.

3. THE PARTIALLY VISIBLE SUN

As described in Section 1, we only observe a third of the Sun's surface, diminishing our ability to isolate individual modes. To take this into account, we use the leakage matrix $L_{\ell m}^{\ell' m'}$, whose action is described thus,

$$\phi_{\ell m}(\omega) = \sum_{\ell' m'} L_{\ell m}^{\ell' m'} a_{\ell' m'}(\omega), \tag{21}$$

where $a_{\ell' m'}(\omega)$ denotes the 'true' oscillations of mode (ℓ', m', n), i.e. for $\omega \approx \omega_{\ell' m' n}$ and $\phi_{\ell m}(\omega)$ the observed oscillations. Note that the leakage matrix is a function of radial order but we do not explicitly state n since we use frequency as a proxy for radial order and also ω always lies within a few linewidths of resonance (Eq. [14]). In the calculations that follow, we use a standard leakage matrix that takes into account line-of-sight projection, limb darkening and comprises both horizontal and radial terms. We note that because we must now distinguish between 'true' and observed oscillations, we will need to correspondingly consider 'true' and observed b coefficients, denoted by B_{st}^σ and b_{st}^σ respectively.

Thus, given a true state of mode coupling, instrumental and other systematics corrupt our retrieved estimates of b coefficients. There is no way to correct for this since the observations are incomplete. The best we can hope to accomplish is to model the systematic effects, mitigate them and appreciate the actual information content of our measurements. Applying the definition of the b coefficient from equation (13) and keeping in mind that we are now dealing with observations, we obtain

$$B_{st}^\sigma(n, \ell) = N_{\ell st}^\sigma \sum_{m, \omega} \gamma_{tm}^{\ell s \ell} H_{\ell \ell m t}^{\sigma *}(\omega) \phi_{\ell m}^*(\omega) \phi_{\ell, m+t}(\omega + \sigma), \tag{22}$$

$$N_{n \ell st}^\sigma = \frac{1}{\sum_{m, \omega} |H_{\ell \ell m t}^\sigma \gamma_{tm}^{\ell s \ell}|^2}, \tag{23}$$

where the summation over frequency follows the interval described in equation (14). Introducing the leakage relation (21) into equation (22), we obtain a significantly bulkier expression,

$$B_{st}^\sigma = N_{\ell st}^\sigma \sum_{\ell', \ell'', m', m'', \omega} L_{\ell m}^{\ell' m'} L_{\ell m + t}^{\ell'' m' + t'} \gamma_{tm}^{\ell s \ell} H_{\ell \ell m t}^{\sigma *} a_{\ell' m'}^{\omega *} a_{\ell'' m''}^{\omega + \sigma}, \tag{24}$$

where a denotes the true wavefield. Substituting equation (12) that relates the true wavefield correlation to the corresponding true b coefficients,

$$a_{\ell' m'}^{\omega *} a_{\ell'' m' + t'}^{\omega + \sigma} = \sum_{s' t'} \gamma_{t' m'}^{\ell'' s' \ell'} H_{\ell' \ell'' m' t'}^\sigma b_{s' t'}^\sigma(\ell', \ell''). \tag{25}$$

Replacing the wavefield correlation on the right-hand side of equation (24) with (25), we obtain

$$B_{st}^{\sigma} = N_{\ell st}^{\sigma} \sum_{\ell', \ell'', m, m', s', t', \omega} L_{\ell m}^{\ell' m'} L_{\ell m+t}^{\ell'' m'+t'} \gamma_{tm}^{\ell s \ell} H_{\ell \ell m t}^{\sigma *} \gamma_{t'm'}^{\ell'' s' \ell'} H_{\ell' \ell'' m' t'}^{\sigma} b_{s't'}^{\sigma}(\ell', \ell''). \tag{26}$$

Equation (26) tells us that the observed B coefficient is a mixture of b-coefficients at several spatial wavenumbers, and it may therefore not be possible to cleanly separate features at different wavenumbers. The degree of this mixing is however mitigated by the leakage terms and $H_{\ell' \ell'' m' t}^{\sigma}$, which represents Lorentzians centred around the mode frequencies $\omega_{n\ell m}$ and $\omega_{n\ell m+t}$. As distances $|\ell'' - \ell|, |\ell' - \ell|, |m' + t' - m|$ and $|m' - m|$ grow, the H factors and leakage matrices fall ever more rapidly. It now bears remembering that the true $b_{s't'}^{\sigma}(\ell', \ell'')$ coefficient no longer contains contributions only from modes of spherical-harmonic degree ℓ - rather, it is from modes ℓ' and ℓ'' with the possibility that $\ell' \neq \ell''$. This implies that the measured B coefficient is sensitive to both toroidal *and* poloidal flows (see Eqs. [6] and [7]). Substituting equation (15) into (26), we obtain

$$B_{st}^{\sigma} = N_{\ell st}^{\sigma} \sum_{\ell', \ell'', m, m', s', t', \omega} L_{\ell m}^{\ell' m'} L_{\ell m+t}^{\ell'' m'+t'} \gamma_{tm}^{\ell s \ell} H_{\ell \ell m t}^{\sigma *} \gamma_{t'm'}^{\ell'' s' \ell'} H_{\ell' \ell'' m' t'}^{\sigma} \times$$

$$\left[g_{\ell'-\ell'',s'} \int_{\odot} dr \, u_{s't'}(r, \sigma) \mathcal{K}_{n\ell}(r) + f_{\ell'-\ell'',s'} \int_{\odot} dr \, w_{s't'}(r, \sigma) \mathcal{K}_{n\ell}(r) \right], \tag{27}$$

where we recall that $|\ell' - \ell''| \ll \ell, s'$. Combining mode-coupling measurements at different radial orders and harmonic degrees, i.e. multiplying both sides by $\alpha^{n\ell}$ as in Section 2.1, and summing over n and ℓ, we obtain an elegant result

$$\beta_{st}^{\sigma}(\sigma) = \sum_{n\ell} \alpha^{n\ell} B_{st}^{\sigma} = \int_{\odot} dr \sum_{s', t'} P_{st}^{s't'}(r, \sigma) u_{s't'}(r, \sigma) + T_{st}^{s't'}(r, \sigma) w_{s't'}(r, \sigma), \tag{28}$$

where

$$P_{st}^{s't'}(r, \sigma) = \sum_{\ell, n} \alpha^{n\ell} \, \Pi_{st}^{s't'}(n, \ell, \sigma), \tag{29}$$

$$\Pi_{st}^{s't'}(n, \ell, \sigma) = N_{\ell st}^{\sigma} \mathcal{K}_{n\ell}(r) \sum_{\ell', \ell'', m, m', \omega} g_{\ell''-\ell',s} L_{\ell m}^{\ell' m'} L_{\ell m+t}^{\ell'' m'+t'} \gamma_{tm}^{\ell s \ell} H_{\ell \ell m t}^{\sigma *} \gamma_{t'm'}^{\ell'' s' \ell'} H_{\ell' \ell'' m' t'}^{\sigma}, \tag{30}$$

$$T_{st}^{s't'}(r, \sigma) = \sum_{\ell, n} \alpha^{n\ell} \, \Theta_{st}^{s't'}(n, \ell, \sigma). \tag{31}$$

$$\Theta_{st}^{s't'}(n, \ell, \sigma) = N_{\ell st}^{\sigma} \mathcal{K}_{n\ell}(r) \sum_{\ell', \ell'', m, m', \omega} f_{\ell''-\ell',s} L_{\ell m}^{\ell' m'} L_{\ell m+t}^{\ell'' m'+t'} \gamma_{tm}^{\ell s \ell} H_{\ell \ell m t}^{\sigma *} \gamma_{t'm'}^{\ell'' s' \ell'} H_{\ell' \ell'' m' t'}^{\sigma}. \tag{32}$$

Note that, in principle, P and T are complex functions, mixing both amplitude and phases of the underlying turbulent velocities. In practice, the imaginary component is smaller by at least 3 orders in magnitude so we may treat P and T as real. This is primarily due to the fact that the leakage matrix is purely real, and may not be fully accounting for all systematical issues (see also Section 5.1, related to the leakage matrix). The terms within square brackets are highlighted since they denote functions purely of ℓ, n, s, s', t, and t'. If the entire Sun were visible, the highlighted terms would be $\propto \delta_{s,s'} \delta_{t,t'}$.

4. SUBTRACTIVE OPTIMALLY LOCALIZED AVERAGING (SOLA)

SOLA is a useful technique with which to incorporate a variety of constraints while limiting the noise level on the eventual inference (Pijpers & Thompson 1994). The combination of measurements results in a corresponding combination of the associated kernels, termed here as the "averaging kernel". In the present problem, we require the averaging kernel sensitive to a given flow wavenumber (s, t) be localized around a given depth, that it possess no surface tail. Additionally, the problem of leakage, described earlier, results in an inability to isolate a single (s, t) mode. Consequently, we penalize kernels sensitive to flows at neighbouring wavenumbers $(s', t') \neq (s, t)$. These three constraints form the SOLA problem relevant to mode coupling. The translation of this into a mathematical form requires solving the following minimization problem

$$\chi_{st} = \frac{1}{2} \int_{\odot} dr \left[T_{st}^{st} - \mathcal{T}(r) \right]^2 + \frac{\lambda}{2} \int_{\odot} dr \sum_{s',t'} \left(T_{st}^{s't'} \right)^2 + \frac{\nu}{2} \int_{\odot} dr f(r) \sum_{s',t'} \left(T_{st}^{s't'} \right)^2, \qquad (33)$$

where $\mathcal{T}(r)$ is the target function, $T_{st}^{s't'}$ is defined in equation (31) and depends on $\alpha_{n\ell}$, which are parameters that are used to combine the modes. The function $f(r)$ is applied to penalise surface tails of the the averaging kernel T_{st}^{st} (see appendix E for a description of function $f(r)$). With the noise model described in Section 5, it is also possible to add a regularization term to control the eventual noise in the inferences. For the moment, we do not include this term but a description of it may be found in e.g. Pijpers & Thompson (1994).

The sum over $(s', t') \neq (s, t)$ penalizes the sensitivity of the measurement combination to flows at neighbouring undesired wavenumbers. The parameters λ and ν are for regularization and must be determined through trial and error (for instance, the optimum choice is commonly associated with the knee of penalty function, when plotted as a function of the noise regularization parameter). To obtain optimal coefficients $\{\alpha\}$, we differentiate χ_{st} with respect to a specific $\alpha_{n\ell}$ and set it to zero,

$$\frac{\partial \chi_{st}}{\alpha_{n\ell}} = \sum_{n'\ell'} \left[\int_{\odot} dr \, \Theta_{st}^{st}(r; n, \ell, \sigma) \, \Theta_{st}^{st}(r; n', \ell', \sigma) \right.$$

$$\left. + [\lambda + \nu f(r)] \sum_{s',t'} \Theta_{st}^{s't'}(r; n, \ell, \sigma) \, \Theta_{st}^{s't'}(r; n', \ell', \sigma) \right] \alpha^{n'\ell'} = \int_{\odot} dr \, \Theta_{st}^{st}(r; n, \ell, \sigma) \, \mathcal{T}(r), \qquad (34)$$

where $(s', t') \neq (s, t)$. Defining matrix A whose matrix elements are given by

$$A_{n\ell,n'\ell'} = \int_{\odot} dr \, \Theta_{st}^{st}(r; n, \ell, \sigma) \, \Theta_{st}^{st}(r; n', \ell', \sigma) + [\lambda + \nu f(r)] \sum_{s',t'} \Theta_{st}^{s't'}(r; n, \ell, \sigma) \, \Theta_{st}^{s't'}(r; n', \ell', \sigma), \quad (35)$$

and the column vector $\{R\}$,

$$R_{n\ell} = \int_{\odot} dr \, \Theta_{st}^{st}(r; n, \ell, \sigma) \, \mathcal{T}(r), \qquad (36)$$

we can obtain the vector of coefficients $\{\alpha_{n\ell}\}$ through a linear least-squares solution $\{\alpha^{n\ell}\} = (A^T A)^{-1} A^T R$ or through methods such as Singular Value Decomposition (SVD). As an aside, we employ SVD here and cut off singular values less than 10^{-5} times the largest singular value.

The primary effect of not penalizing leakage in the (s, t) space as described in equation (33) is shown in Figures 1 and 3. A naive sum over B coefficients shows dominant surface sensitivity to
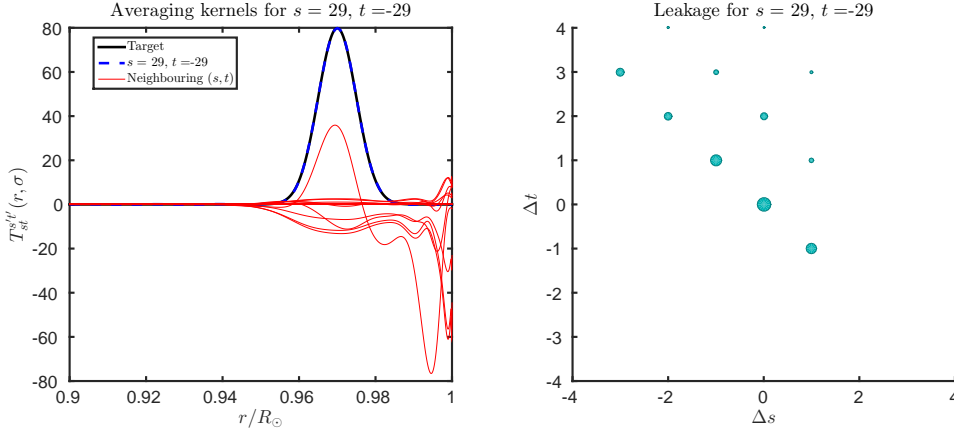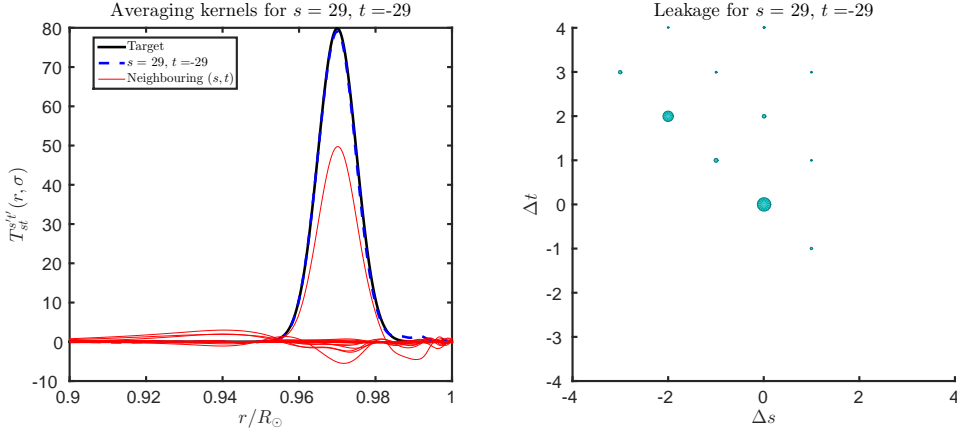
Figure 1. On the left plot, we show an attempt at summing up measurements (and therefore the kernels) to image convective velocities at spatial wavenumber $(s,t) = (29,-29)$ at a depth of $r/R_\odot = 0.97$. The black (thick solid) line is the (desired) target Gaussian. Limited viewing of the Sun results in the inability to isolate individual spherical harmonic oscillation modes, which in turn translates into blurring of the spatial (s,t) domain of perturbations. In this case, we set $\lambda = 0 = \nu$ in equation (33), i.e. no leakage penalties. As a consequence, adjacent (s,t) wavenumbers (thin red lines) contribute substantially to the desired inference at $(s,t) = (29,-29)$ (thick blue dashed line; indistinguishable from the black solid line). If the Sun were to be fully visible, the thin red lines would vanish and we would only see the the dashed blue and target Gaussian lines. On the right plot, the leakage is shown pictorially; the big blue dot at $(\Delta s, \Delta t) = (0,0)$ corresponds to the energy associated with the desired (29,-29) mode whereas all other dots denote leakage from adjacent wavenumbers. Indeed, full-Sun coverage would result in an empty plot with a single dot in the centre. Note that the problem of leakage appears to be less severe in this case than in Figure 3, since the constraint $|t + \Delta t| \leq s + \Delta s$ limits the number of modes into which leakage can occur.

neighbouring (s,t) wavenumbers and weak sensitivity to the wavenumber of interest. In particular, the (undesired) neighbouring-wavenumber sensitivity overwhelms the desired $(s,t) = (21,15)$ sensitivity, thereby rendering interpretation infeasible. This is not altogether surprising since kernels for all helioseismic measurements have strong surface sensitivity (the 'shower-glass effect', as described by Schunker et al. 2005) and it typically requires careful analysis to remove the surface contribution. The penalties in equation (33) accomplish the tasks of limiting the sensitivity to neighbouring wavenumbers (λ term) and the overall surface sensitivity (ν term). We find empirically that $\lambda = 0$ with finite ν works well for imaging relatively deep layers (i.e. $r/R_\odot < 0.98$ for instance) whereas when imaging the immediate sub-surface, i.e. $r/R_\odot = 0.99$, we set $\nu = 0$ and apply a finite λ. We show cases for imaging at the depth $r/R_\odot = 0.97$ for two different wavenumbers in Figures 2 and 4.

Because power from neighbouring wavenumbers leak into the channel we seek to infer, we normalize the $\alpha_{n\ell}$ coefficients thus

$$\alpha_{n\ell} \to \frac{\alpha_{n\ell}}{\sqrt{\left(\sum_{s't'} \int_\odot dr\, T_{st}^{s't'}\right)^2}}. \tag{37}$$

Figure 2. On the left plot, we show an attempt at summing up measurements (and therefore the kernels) to image convective velocities at spatial wavenumber $(s,t) = (29, -29)$ at a depth of $r/R_\odot = 0.97$. The black solid line is the (desired) target Gaussian. Limited viewing of the Sun results in the inability to isolate individual spherical harmonic oscillation modes, which in turn translates into blurring of the spatial (s,t) domain of perturbations. For the leakage penalties, we choose $\lambda = 0, \nu = 0.5$ in equation (33). Therefore the contribution from neighbouring (s,t) wavenumbers (thin red lines) to the desired inference at $(s,t) = (29, -29)$ (the blue dashed line) is much weaker than in Figure 1. If the Sun were to be fully visible, the thin red lines would vanish and we would only see the the dashed blue and target Gaussian lines. On the right plot, the leakage is shown pictorially; the big blue dot at $(\Delta s, \Delta t) = (0, 0)$ corresponds to the energy associated with the desired (29,-29) mode whereas all other dots denote leakage from neighbouring wavenumbers. Note that since $|t + \Delta t| \leq s + \Delta s$, the dots do not cover the entire map.

Finally, the average flow component $w_{st}(r_0, \sigma)$ is given by

$$w_{st}(r_0, \sigma) \approx \int_\odot dr \, T^{st}_{st}(r, \sigma) \, w_{st}(r, \sigma) = \sum_{n\ell} \alpha^{nl} B_{st}(n, \ell, \sigma). \tag{38}$$

5. NOISE MODEL

Correlated realization noise forms a significant fraction of measurement. Accurate inference of the underlying convective flows requires that we model the contribution from correlated noise to B coefficients. The analysis may be extended to correlations across different harmonic degrees as well. Following the notation of Woodard (2016),
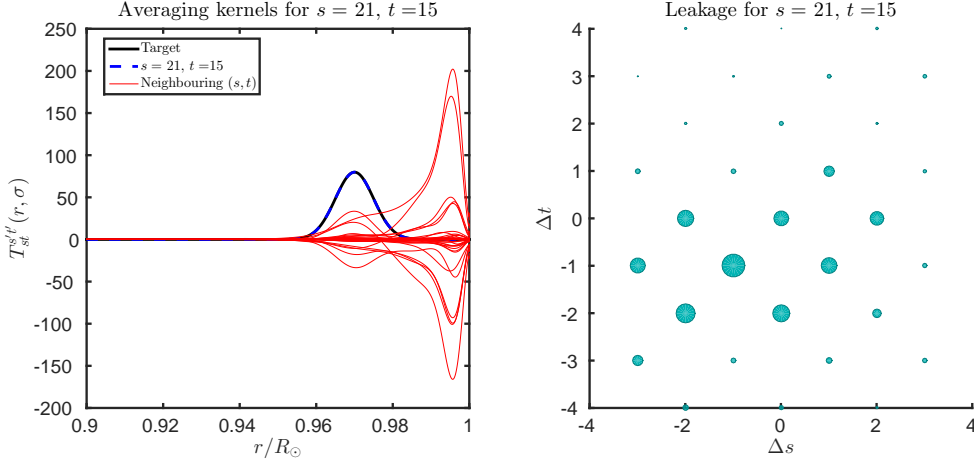
$$B^\sigma_{st}(\ell) = \frac{\sum_{m,\omega} G^{st*}_{\ell m\omega} \phi^{\omega*}_{\ell m} \phi^{\omega+\sigma}_{\ell m+t}}{\sum_{m,\omega} |G^{st}_{\ell m\omega}|^2}, \tag{39}$$

where G is defined thus

$$G^{st}_{\ell m\omega} = L^{\ell m}_{\ell m} L^{\ell m+t}_{\ell m+t} H^\sigma_{\ell\ell mt} \gamma^{\ell s\ell}_{tm}. \tag{40}$$

Note that this is the same as in equation (22), except that only diagonal leakage terms are now included. We model $\phi^\omega_{\ell m}$ as a multi-variate Gaussian random process with the following property (e.g. Woodard 1997; Gizon & Birch 2004),

$$\langle \phi^{\omega*}_{\ell m} \phi^{\omega'}_{\ell m+t} \rangle = \delta_{\omega,\omega'} \langle \phi^{\omega*}_{\ell m} \phi^\omega_{\ell m+t} \rangle. \tag{41}$$

Figure 3. On the left plot, we show an attempt at summing up measurements (and therefore the kernels) to image convective velocities at spatial wavenumber $(s, t) = (21, 15)$ at a depth of $r/R_\odot = 0.97$. The black (thick solid) line is the (desired) target Gaussian. Limited viewing of the Sun results in the inability to isolate individual spherical harmonic oscillation modes, which in turn translates into blurring of the spatial (s, t) domain of perturbations. In this case, we set $\lambda = 0 = \nu$ in equation (33), i.e. no leakage penalties. Contributions from neighbouring (s, t) wavenumbers (thin red lines) are seen to overwhelm the desired inference at $(s, t) = (21, 15)$ (thick blue dashed line; indistinguishable from the black solid line). If the Sun were to be fully visible, the thin red lines would vanish and we would only see the the dashed blue and target Gaussian lines. On the right plot, the leakage is shown pictorially; the big blue dot at $(\Delta s, \Delta t) = (0, 0)$ corresponds to the energy associated with the desired (21,15) mode whereas all other dots denote leakage from adjacent wavenumbers. With penalties described in equation (33), the problem of leakage can be greatly mitigated and the inference can be focused on the desired wavenumber and radius, apparent in Figure 4.

Let us first consider the contribution of pure noise to the B coefficient by studying the expectation value of equation (39),
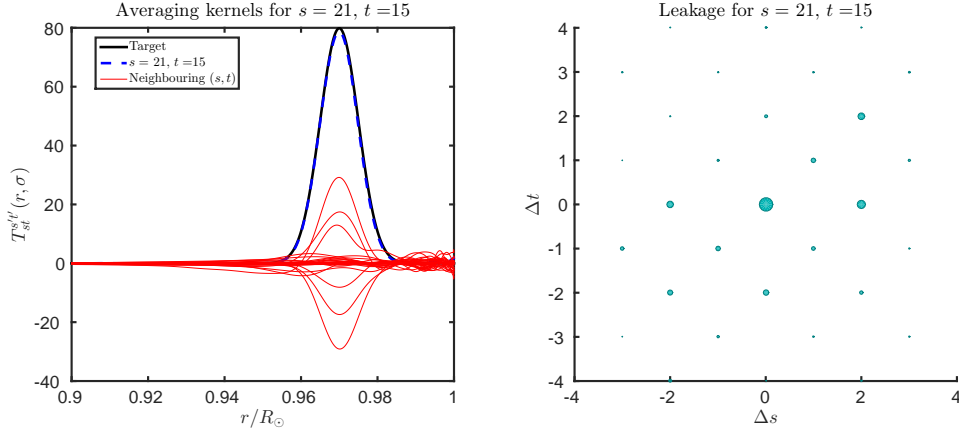
$$\langle B_{st}^\sigma \rangle = \frac{\sum_{m,\omega} G_{\ell m\omega}^{st*} \langle \phi_{\ell m}^{\omega*} \phi_{\ell m+t}^{\omega+\sigma} \rangle}{\sum_{m,\omega} |G_{\ell m\omega}^{st}|^2} = \frac{\sum_{m,\omega} G_{\ell m\omega}^{st*} \langle \phi_{\ell m}^{\omega*} \phi_{\ell m+t}^{\omega} \rangle \delta_{\sigma 0}}{\sum_{m,\omega} |G_{\ell m\omega}^{st}|^2}, \tag{42}$$

which is therefore trivial except at $\sigma = 0$. Now let us study the second moment (i.e. the variance) of B

$$\langle |B_{st}^\sigma|^2 \rangle = \frac{\sum_{m,m',\omega,\omega'} G_{\ell m\omega}^{st*} G_{\ell m'\omega'}^{st} \langle \phi_{\ell m}^{\omega*} \phi_{\ell m+t}^{\omega+\sigma} \phi_{\ell m'}^{\omega'} \phi_{\ell m'+t}^{\omega'+\sigma*} \rangle}{[\sum_{m,\omega} |G_{\ell m\omega}^{st}|^2]^2}. \tag{43}$$

Isserlis' theorem (Isserlis 1918) states that the following relationship governs fourth moments of multivariate zero-mean Gaussian processes X_i:

$$\langle X_1 X_2 X_3 X_4 \rangle = \langle X_1 X_2 \rangle \langle X_3 X_4 \rangle + \langle X_1 X_3 \rangle \langle X_2 X_4 \rangle + \langle X_1 X_4 \rangle \langle X_2 X_3 \rangle. \tag{44}$$

Figure 4. On the left plot, we show an attempt at summing up measurements (and therefore the kernels) to image convective velocities at spatial wavenumber $(s, t) = (21, 15)$ at a depth of $r/R_\odot = 0.97$. The black (thick solid) line is the (desired) target Gaussian. Limited viewing of the Sun results in the inability to isolate individual spherical harmonic oscillation modes, which in turn translates into blurring of the spatial (s, t) domain of perturbations. In contrast to Figure 4, we apply leakage penalties by setting $\lambda = 0, \nu = 0.5$ in equation (33). While a variety of neighbouring (s, t) wavenumbers (thin red lines) contribute to the desired inference at $(s, t) = (21, 15)$ (thick blue dashed line), they all show power in the desired depth range and there is no surface sensitivity as was the case in Figure 4. If the Sun were to be fully visible, the thin red lines would vanish and we would only see the the dashed blue and target Gaussian lines. On the right plot, the leakage is shown pictorially; the big blue dot at $(\Delta s, \Delta t) = (0, 0)$ corresponds to the energy associated with the desired (21,15) mode whereas all other dots denote leakage from neighbouring wavenumbers. When comparing with Figure 4, it is seen that the leakage is substantially mitigated through the application of penalties.

Applying equation (44) to (43), we arrive at

$$\langle |B_{st}^\sigma|^2 \rangle = \left[\sum_{m,\omega} |G_{\ell m \omega}^{st}|^2 \right]^{-2} \sum_{m,m',\omega,\omega'} G_{\ell m \omega}^{st*} G_{\ell m'\omega'}^{st} \left(\langle \phi_{\ell m}^{\omega *} \phi_{\ell m+t}^{\omega+\sigma} \rangle \langle \phi_{\ell m'}^{\omega'} \phi_{\ell m'+t}^{\omega'+\sigma *} \rangle + \right.$$
$$\left. \langle \phi_{\ell m}^{\omega *} \phi_{\ell m'}^{\omega'} \rangle \langle \phi_{\ell m+t}^{\omega+\sigma} \phi_{\ell m'+t}^{\omega'+\sigma *} \rangle + \langle \phi_{\ell m}^{\omega *} \phi_{\ell m'+t}^{\omega'+\sigma *} \rangle \langle \phi_{\ell m'}^{\omega'} \phi_{\ell m'+t}^{\omega+\sigma} \rangle \right).$$

The first term resembles equation (42) and therefore only contributes at $\sigma = 0$, which is of no interest. The second term is

$$\langle \phi_{\ell m}^{\omega *} \phi_{\ell m'}^{\omega'} \rangle \langle \phi_{\ell m+t}^{\omega+\sigma} \phi_{\ell m'+t}^{\omega'+\sigma *} \rangle = \delta_{\omega,\omega'} \langle \phi_{\ell m}^{\omega *} \phi_{\ell m'}^{\omega} \rangle \langle \phi_{\ell m+t}^{\omega+\sigma} \phi_{\ell m'+t}^{\omega+\sigma *} \rangle. \tag{45}$$

The third term, like the first, is also trivial since over the summation interval $\omega, \omega' > 0$, $\langle \phi_{\ell m'}^{\omega'} \phi_{\ell m+t}^{\omega+\sigma} \rangle = 0$.

The noise model for the variance of B coefficients is therefore

$$\langle |B_{st}^\sigma|^2 \rangle = \frac{\sum_{m,m',\omega} G_{\ell m \omega}^{st*} G_{\ell m'\omega}^{st} \langle \phi_{\ell m}^{\omega *} \phi_{\ell m'}^{\omega} \rangle \langle \phi_{\ell m+t}^{\omega+\sigma} \phi_{\ell m'+t}^{\omega+\sigma *} \rangle}{[\sum_{m,\omega} |G_{\ell m \omega}^{st}|^2]^2}. \tag{46}$$

Considering the impact of leakage, we have

$$\langle \phi_{\ell m}^{\omega *} \phi_{\ell m'}^{\omega} \rangle = \sum_{\ell' p\, \ell'' p'} L_{\ell m}^{\ell' p} L_{\ell m'}^{\ell'' p'} a_{\ell' p}^{\omega *} a_{\ell'' p'}^{\omega *} = \sum_{\ell' p\, \ell'' p'} L_{\ell m}^{\ell' p} L_{\ell m'}^{\ell'' p'} N_p \, \delta_{\ell' \ell''} \, \delta_{p' p} \, |R_{\ell' p}^{\omega}|^2$$

$$= \sum_{\ell' p} L_{\ell m}^{\ell' p} L_{\ell m'}^{\ell' p} N_{\ell'} \, |R_{\ell' p}^{\omega}|^2. \qquad (47)$$

5.1. *Incomplete model of noise*

A fundamental problem with the noise model becomes apparent upon further analysis of equation (47). The observed wavefield $\phi_{\ell m}^{\omega}$ is complex and so is its correlation. The imaginary and real parts of $\phi_{\ell m}^{\omega *} \phi_{\ell m'}^{\omega}$ directly computed from data are comparable in magnitude. However the model on the right-hand side of equation (47) is real since the leakage matrix can be chosen to be real with no loss of generality (e.g. Schou & Brown 1994). The imaginary component of the wavefield correlation would therefore be interpreted as comprising entirely of signal, which is likely not the case. Thus there are missing ingredients in the model, or perhaps the leakage matrix, and determining what these are exactly is a focus of future work. For the purposes of the present analysis, we make the following assumption,

$$\langle \phi_{\ell m}^{\omega *} \phi_{\ell m'}^{\omega} \rangle = \langle |\phi_{\ell m}^{\omega}|^2 \rangle \, \delta_{mm'} = \sum_{\ell' p} (L_{\ell m}^{\ell' p})^2 N_{\ell'} \, |R_{\ell' p}^{\omega}|^2, \qquad (48)$$

which then ensures that two sides of the equation are consistent, giving us the following noise model,

$$\langle |B_{st}^{\sigma}|^2 \rangle = \frac{\sum_{m,\omega} |G_{\ell m \omega}^{st}|^2 \langle |\phi_{\ell m}^{\omega}|^2 \rangle \langle |\phi_{\ell m+t}^{\omega + \sigma}|^2 \rangle}{[\sum_{m,\omega} |G_{\ell m \omega}^{st}|^2]^2}. \qquad (49)$$

5.2. *Estimating signal (flow) power*

The analysis set out in Section 4 along with this noise model describes how to subtract noise from B-coefficients, i.e.

$$\text{signal} = \left| \sum_{n,\ell} \alpha_{n\ell} \, B_{st}^{\sigma}(n,\ell) \right|^2 - \sum_{n,\ell} \alpha_{n\ell}^2 \langle |B_{st}^{\sigma}(n,\ell)|^2 \rangle, \qquad (50)$$

where the left-hand side is the signal, the first term on the right-hand side represents the squared absolute value of the weighted sum of the observed B coefficients and the second term is the weighted sum of the expected noise for each coefficient. Note that the variance in the power ('noise of the noise') quantifies the expected error bars on the inferences of the signal. This requires evaluating an eighth moment of the wavefield, and the calculation is outlined in appendix B. At present, we have not evaluated these terms. In Figures 5, 6 and 7, we plot the B-coefficient and noise power as functions of temporal frequency σ and harmonic degree s. The observed B-coefficients were computed for specific oscillation modes (described in the attendant captions) from 1 year of Michelson Doppler Imager observations (1996 -1997; Scherrer et al. 1995). In Figure 5, the noise model and B-coefficient power are essentially consistent with each other whereas in Figures 6 and 7, B-coefficient power is notably larger than the theoretically predicted noise level (Eq. [49]).
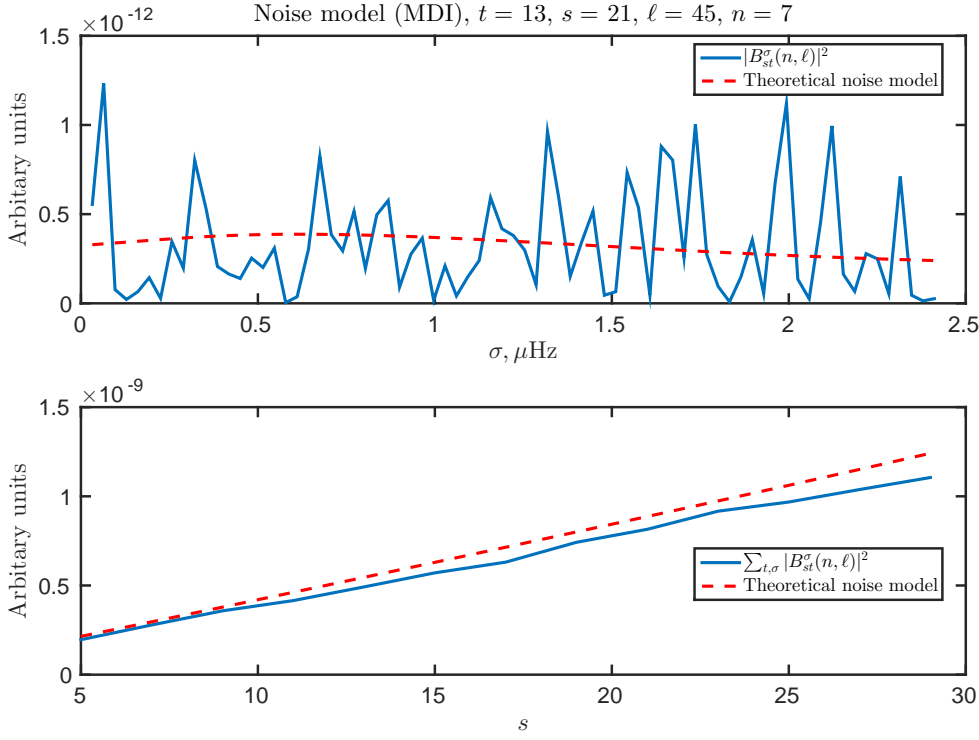
Figure 5. Noise model for Michelson-Doppler-Imager (MDI) measurements of normal-mode coupling B^σ_{st} from one year's data, obtained from the $\ell = 45, n = 7$ mode. Upper panel: the solid blue line shows $|B^\sigma_{st}|^2$ as a function of frequency σ at a specific $(s,t) = (21, 13)$ and the dashed red line is the theoretical noise model in equation (49). It is seen that the theoretical noise model broadly captures the variance of the $|B^\sigma_{st}|^2$ curve except perhaps at high frequencies. Lower panel: Both curves summed over t and σ and plotted as a function of harmonic degree s. This curve suggests that the power in $|B^\sigma_{st}|^2$ is essentially consistent with realization noise.

6. CONCLUSIONS

We have studied the problem of how to best combine wavefield-correlation measurements in the Sun in order to obtain optimal inferences of desired properties in the solar interior. These correlations are measured from observations using a linear-least-squares methodology described in e.g. Woodard (2016). A great benefit of using this technique is that it is a linear functional of the wavefield, unlike the non-linear least squares approach adopted by e.g. Schou (1992) to obtain global-mode parameters. There is a downside to adopting a straightforward method, namely that spatial leakage between oscillation modes is transmitted directly to a leakage between wavenumbers of the perturbation. Thus it might ostensibly be difficult to isolate individual spherical-harmonic wavenumbers of the perturbation. As a first step, we derive the sensitivities of the normal-mode-coupling measurement (specifically the so-called B coefficient) to perturbations, finding that, in addition to being dominantly sensitive to (s,t) it is also sensitive to adjacent wavenumbers, i.e.
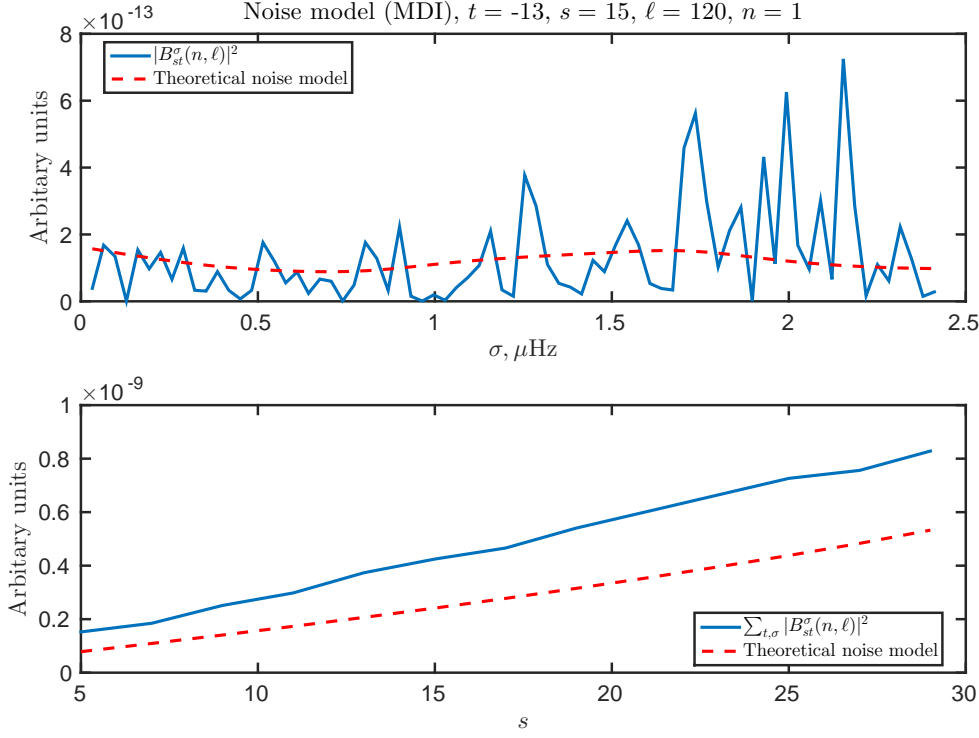
Figure 6. Noise model for MDI measurements of normal-mode coupling B_{st}^{σ} from one year's data, obtained from the $\ell = 120, n = 1$ mode. Upper panel: the solid blue line shows $|B_{st}^{\sigma}|^2$ as a function of frequency σ at a specific $(s,t) = (15, -13)$, the dashed red line is the theoretical noise model in equation (49). Lower panel: The noise and signal summed over t and σ and plotted as a function of harmonic degree s. In contrast to Figure 5, it is seen that the theoretical model predicts a much lower noise level than the $|B_{st}^{\sigma}|^2$ curve, suggesting the existence of signal in this (s,t) channel as sensed by $\ell = 120, n = 1$.

within the range $(s\pm2, t\pm2)$. The question of how to optimally combine the measured B coefficients such that it is overwhelmingly sensitive only to the (s,t) wavenumber while being sharply localized at a desired depth (and no surface tail) and also ensuring that noise level of the inferred flow velocity is reasonable. To that end, we build a noise model for B coefficients, which can then be propagated to the inferred flow velocities. We find (to our pleasant surprise) that when combining a sufficient number of modes, all these constraints are well met. The issue of leakage suggests that the convective-velocity-amplitude estimates of Woodard (2016), which were obtained by direct sums over harmonic degree, are associated with surface layers (as opposed to the interior) and may therefore explain why they are relatively large. Overall, the present results strongly encourage a more complete exploration of the possibilities of using normal-mode coupling to infer the internal properties of the Sun.
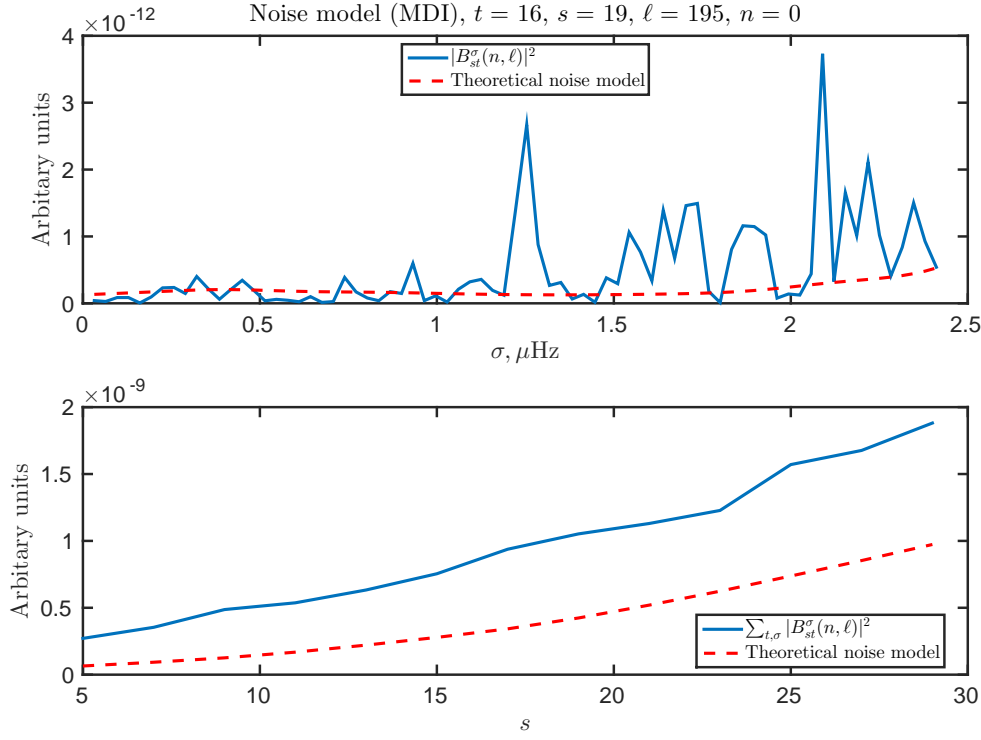
Figure 7. Noise model for MDI measurements of normal-mode coupling B_{st}^{σ} from one year's data, obtained from the $\ell = 195, n = 0$ mode. Upper panel: the solid blue line shows $|B_{st}^{\sigma}|^2$ as a function of frequency σ at a specific $(s, t) = (15, -13)$, the dashed red line is the theoretical noise model in equation (49). Lower panel: The noise and signal summed over t and σ and plotted as a function of harmonic degree s. In contrast to Figure 5 and similar to Figure 6, it is seen that the theoretical model predicts a much lower noise level than the $|B_{st}^{\sigma}|^2$ curve, suggesting the existence of signal in this (s, t) channel as sensed by $\ell = 195, n = 0$.

REFERENCES

Christensen–Dalsgaard, J. 2003, Lecture Notes on Stellar Oscillations, 5th edn.

Christensen-Dalsgaard, J. 2002, Reviews of Modern Physics, 74, 1073

Christensen-Dalsgaard, J., Dappen, W., Ajukov, S. V., Anderson, E. R., Antia, H. M., Basu, S., Baturin, V. A., Berthomieu, G., Chaboyer, B., Chitre, S. M., Cox, A. N., Demarque, P., Donatowicz, J., Dziembowski, W. A., Gabriel, M., Gough, D. O., Guenther, D. B., Guzik, J. A., Harvey, J. W., Hill, F., Houdek, G., Iglesias, C. A., Kosovichev, A. G., Leibacher, J. W., Morel, P., Proffitt, C. R., Provost, J., Reiter, J., Rhodes, Jr., E. J., Rogers, F. J., Roxburgh, I. W., Thompson, M. J., & Ulrich, R. K. 1996, Science, 272, 1286

Cutler, C. 2017, ArXiv e-prints

Dahlen, F. A., & Tromp, J. 1998, Theoretical Global Seismology (Princeton University Press)

Gizon, L., & Birch, A. C. 2004, ApJ, 614, 472

Gizon, L., Birch, A. C., & Spruit, H. C. 2010, ARA&A, 48, 289

Hanasoge, S. M. 2017, MNRAS, 470, 2780

Hanasoge, S. M., Woodard, M., Antia, H. M., Gizon, L., & Sreenivasan, K. R. 2017, MNRAS, 470, 1404

Isserlis, L. 1918, Biometrika, 12, 134

Lavely, E. M., & Ritzwoller, M. H. 1992, Philosophical Transactions of the Royal Society of London Series A, 339, 431

Pijpers, F. P., & Thompson, M. J. 1994, A&A, 281, 231

Schad, A., Timmer, J., & Roth, M. 2011, ApJ, 734, 97

Scherrer, P. H., Bogart, R. S., Bush, R. I., Hoeksema, J. T., Kosovichev, A. G., Schou, J., Rosenberg, W., Springer, L., Tarbell, T. D., Title, A., Wolfson, C. J., Zayer, I., & MDI Engineering Team. 1995, SoPh, 162, 129

Schou, J. 1992, PhD thesis, , Aarhus University, Aarhus, Denmark, (1992)

Schou, J., & Brown, T. M. 1994, A&AS, 107

Schunker, H., Braun, D. C., Cally, P. S., & Lindsey, C. 2005, ApJL, 621, L149

Vorontsov, S. V. 2011, Monthly Notices of the Royal Astronomical Society, 418, 1146

Woodard, M. 2014, SoPh, 289, 1085

Woodard, M., Schou, J., Birch, A. C., & Larson, T. P. 2013, SoPh, 287, 129

Woodard, M. F. 1997, ApJ, 485, 890

—. 2016, MNRAS, 460, 3292

APPENDIX

A. DERIVATION OF ASYMPTOTIC KERNELS

The kernel sensitive to toroidal flows is given by (Eq. 60 of Hanasoge et al. 2017)

$$K_w^{st} = \frac{\rho r \omega_{n\ell}}{2\sqrt{\pi}} \ell'(\ell'+1)\sqrt{(2\ell'+1)(2\ell+1)}\gamma_{tm}^{\ell's\ell}(1-(-1)^{\ell'+\ell+s})\begin{pmatrix} \ell' & s & \ell \\ -1 & 0 & 1 \end{pmatrix} \times$$

$$(-UU' + VU' + UV' - \frac{VV'}{2}[\ell'(\ell'+1) + \ell(\ell+1) - s(s+1)]), \qquad \text{(A1)}$$

where U, V are eigenfunctions corresponding to spherical-harmonic degree ℓ and similarly for the primed quantities. The phase factor $1 - (-1)^{\ell'+\ell+s}$ constrains the kernel to be non-zero only when $\ell' + s + \ell$ is odd. We use the following asymptotic relation for the Wigner-3j symbol (appendix A, Eq. A3 of Vorontsov 2011)

$$\begin{pmatrix} \ell' & s & \ell \\ -m & 0 & m \end{pmatrix} \approx \frac{(-1)^{\ell'+m}}{\sqrt{2\ell}}\left[\frac{(s-\ell'+\ell)!}{(s+\ell'-\ell)!}\right]^{\frac{1}{2}} P_s^{\ell'-\ell}\left(\frac{m}{\ell}\right), \qquad \text{(A2)}$$

where P_s^ℓ is the associated Legendre polynomial and the approximation is valid in the limit $s \ll \ell, \ell'$. Further assuming that $\ell \approx \ell' \gg 1$ and considering the specific case of $t = 0$ and $m = 1 = m'$, the following approximation is known to apply (appendix A, Eq. A4 of Vorontsov 2011) when $s + \ell' + \ell$ is odd

$$\begin{pmatrix} \ell' & s & \ell \\ -m & 0 & m \end{pmatrix}\begin{pmatrix} \ell' & s & \ell \\ -1 & 0 & 1 \end{pmatrix} \approx (-1)^{\frac{s-\ell'+\ell+2m+1}{2}}\frac{(s-\ell'+\ell)!!(s+\ell'-\ell)!!}{2\ell^2(s+\ell'-\ell)!}P_s^{\ell'-\ell}\left(\frac{m}{\ell}\right). \qquad \text{(A3)}$$

Dividing asymptotic relation (A3) by (A2), we arrive at

$$\begin{pmatrix} \ell' & s & \ell \\ -1 & 0 & 1 \end{pmatrix} \approx (-1)^{\frac{s-\ell'+\ell+1}{2}-\ell'}\frac{(s-\ell'+\ell)!!(s+\ell'-\ell)!!}{\sqrt{2}\ell^{\frac{3}{2}}\sqrt{(s+\ell'-\ell)!(s-\ell'+\ell)!}}. \qquad \text{(A4)}$$

Approximating $U' \approx U, V' \approx V, |UV| \ll |U^2|, \ell(\ell+1)|V^2|, \ell'(\ell'+1)+\ell(\ell+1) \gg s(s+1)$ and $\ell \approx \ell'$, and leaving the Wigner-3j symbols alone for now, we obtain

$$K_w^{st}(r) = -\frac{2}{\sqrt{\pi}}\ell^3\gamma_{tm}^{\ell's\ell}\rho r \omega_{n\ell}\begin{pmatrix} \ell' & s & \ell \\ -1 & 0 & 1 \end{pmatrix}\left[U^2 + \ell(\ell+1)V^2\right]. \qquad \text{(A5)}$$

Substituting the asymptotic expression (A4) for the Wigner-3j symbol, multiplying equation (A5) by $(-1)^{\ell'+\ell'-\ell+\ell}$, replacing the negative sign by $(-1)^{-1}$ and rearranging, we arrive at

$$K_w^{st}(r) \approx (-1)^{\frac{s+\ell'-\ell-1}{2}}(-1)^\ell\ell^{\frac{3}{2}}\sqrt{\frac{2}{\pi}}\gamma_{tm}^{\ell's\ell}\rho r \omega_{n\ell}\left[U^2 + V^2\ell(\ell+1)\right]\frac{(s-\ell'+\ell)!!(s+\ell'-\ell)!!}{\sqrt{(s+\ell'-\ell)!(s-\ell'+\ell)!}}. \qquad \text{(A6)}$$

Note that there is a factor of 2 discrepancy between asymptotic expression (A6) and equations (45) and (46) of Woodard (2014). To confirm that the expressions derived here are correct, we plot the exact and asymptotic expressions for $\ell = 103, n = 7, s = 17$ in Figure 8.
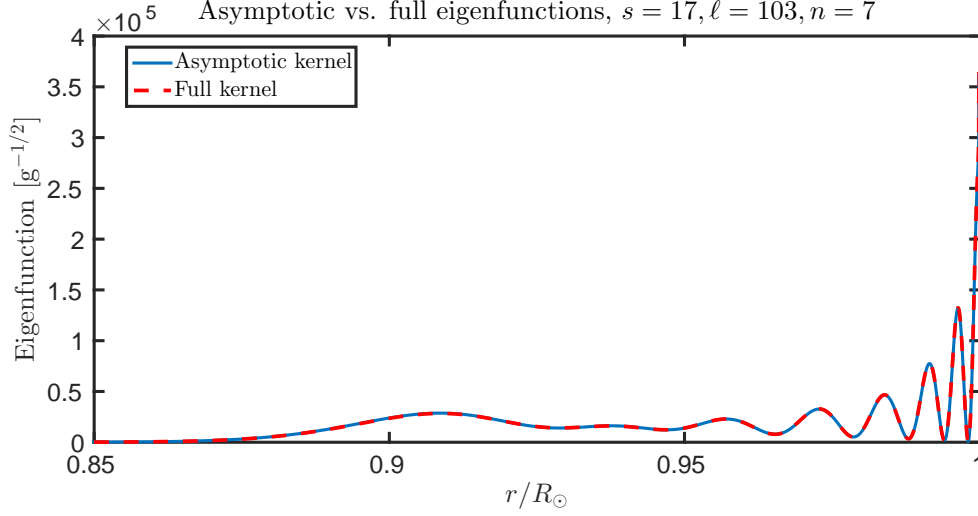
Figure 8. Comparison between exact (Eq. [A1]) and asymptotic (Eq. [A6]) kernels for $\ell = 103, n = 7, s = 17$ plotted as a function of radius. It is seen that these are essentially indistinguishable. Although not shown here, we find that the asymptotic and full expressions for these kernels are remarkably well matched over broad ranges of n, ℓ, s. Note that the comparison gets slightly worse when $s \approx \ell$ but the match even in the worst cases was very good (not shown here).

B. VARIANCE OF THE NOISE

We compute the variance of the noise in order to place error bars on the degree of confidence in bounding the magnitudes of convective velocities. The variance is given by $\langle |B_{st}^{\sigma}|^4 \rangle - \langle |B_{st}^{\sigma}|^2 \rangle^2$ and we need to compute the first term, which is

$$\langle |B_{st}^{\sigma}|^4 \rangle = \frac{\sum G_{\ell m \omega}^{st*} G_{\ell m' \omega'}^{st} G_{\ell m'' \omega''}^{st*} G_{\ell m''' \omega'''}^{st} \langle \phi_{\ell m}^{\omega *} \phi_{\ell m'}^{\omega'} \phi_{\ell m+t}^{\omega+\sigma} \phi_{\ell m'+t}^{\omega'+\sigma *} \phi_{\ell m''}^{\omega'' *} \phi_{\ell m'''}^{\omega'''} \phi_{\ell m''+t}^{\omega''+\sigma} \phi_{\ell m'''+t}^{\omega'''+\sigma *} \rangle}{[\sum_{m,\omega} |G_{\ell m \omega}^{st}|^2]^4},$$
(B7)

where the sum is applied over repeated indices. Invoking Isserlis' theorem, the eighth-order product in equation (B7) is simplified to obtain the following twelve terms

$$\langle |B_{st}^{\sigma}|^4 \rangle = \left[\sum_{m,\omega} |G_{\ell m \omega}^{st}|^2 \right]^{-4} \left[2 \left(\sum_{m,\omega} |G_{\ell m \omega}^{st}|^2 P_{\ell m}^{\omega} P_{\ell m+t}^{\omega+\sigma} \right)^2 + 2 \sum_{m,\omega} |G_{\ell m \omega}^{st}|^4 \left(P_{\ell m}^{\omega} P_{\ell m+t}^{\omega+\sigma} \right)^2 + \right.$$

$$\sum_{m,\omega} 2|G_{\ell m \omega}^{st}|^2 |G_{\ell m-t,\omega-\sigma}^{st}|^2 P_{\ell m-t}^{\omega-\sigma} \left(P_{\ell m}^{\omega} \right)^2 P_{\ell m+t}^{\omega+\sigma} + |G_{\ell m \omega}^{st}|^2 |G_{\ell m+t\omega+\sigma}^{st}|^2 \left(P_{\ell m}^{\omega} \right)^2 P_{\ell m+t}^{\omega+\sigma} P_{\ell m+2t}^{\omega+2\sigma}$$

$$\left. + |G_{\ell m \omega}^{st}|^2 |G_{\ell m+t,\omega+\sigma}^{st} G_{\ell m-t,\omega-\sigma}^{st}| \left(P_{\ell m+t}^{\omega+\sigma} \right)^2 P_{\ell m+2t}^{\omega+2\sigma} P_{\ell m}^{\omega} \right],$$
(B8)

where we define $P_{\ell m}^{\omega} = \langle |\phi_{\ell m}^{\omega}|^2 \rangle$ and $P_{\ell m+t}^{\omega+\sigma} = \langle |\phi_{\ell m+t}^{\omega+\sigma}|^2 \rangle$ and so on. We do not compute this term in the present analysis.

C. ENFORCING PARITY IN B COEFFICIENTS

Flows (and sound-speed perturbations etc.) in the spatial and temporal domain are real, which implies the following relationship for the corresponding coefficients in Fourier domain, $w_{st}(r,\sigma) = (-1)^t w^*_{s,-t}(r,-\sigma)$ (since we consider only toroidal flows in this discussion). Ignoring leakage in (s,t) space, i.e. assuming that the effective kernel T has very little power in the $(s',t') \neq (s,t)$ channels in comparison to (s,t), we obtain

$$\beta^\sigma_{st} \approx \int_\odot dr\, T^{st}_{st}(r,\sigma)\, w_{st}(r,\sigma), \qquad (-1)^t \beta^{-\sigma*}_{s,-t} \approx \int_\odot dr\, T^{s,-t*}_{s,-t}(r,-\sigma)\, [(-1)^t\, w^*_{s,-t}(r,-\sigma)], \quad \text{(C9)}$$

which gives us

$$\frac{\beta^\sigma_{st} + (-1)^t \beta^{-\sigma*}_{s,-t}}{2} = \int_\odot dr\, \frac{T^{st}_{st}(r,\sigma) + T^{s,-t*}_{s,-t}(r,-\sigma)}{2}\, w_{st}(r,\sigma). \tag{C10}$$

suggesting that the correct measurement to make and the appropriate kernel are the averages of the corresponding (t,σ) and $(-t,-\sigma)$ values.

D. MODE NORMALIZATION CONSTANT

The power spectrum of an oscillation mode is given by a Lorentzian (e.g. Schou & Brown 1994),

$$P(\omega) = \frac{P_{\text{tot}}\Gamma_{n\ell}/2}{(\omega - \omega_{n\ell})^2 + (\Gamma_{n\ell}/2)^2}, \tag{D11}$$

and defining $P_{\text{tot}} = C_{n\ell}A^2_{n\ell}/2$, where $A_{n\ell}$ is the measured amplitude of the mode in question and $C_{n\ell}$ is an overall normalization factor described below. From the definition of the power spectrum,

$$\langle|\phi^\omega_{\ell m}|^2\rangle = N_\ell \sum_{\ell' m'} (L^{\ell'm'}_{\ell m})^2 |R^\omega_{\ell'm'}|^2, \tag{D12}$$

where $R^\omega_{\ell m}$ stated in equation (2). Thus the power spectrum is given by

$$\langle|\phi^\omega_{\ell m}|^2\rangle \approx \frac{N_\ell}{4\omega^2_{n\ell}} \sum_{\ell' m'} \frac{(L^{\ell'm'}_{\ell m})^2}{(\omega_{n\ell'm'} - \omega)^2 + (\Gamma_{n\ell}/2)^2}. \tag{D13}$$

Comparing equations (D11) and (D13), we obtain $N_\ell = C_{n\ell}A^2_{n\ell}\omega^2_{n\ell}\Gamma_{n\ell}$, where $C_{n\ell}$ is defined as

$$C_{n\ell} = \frac{\sum_{m,\omega} |\phi^\omega_{\ell m}|^2}{A^2_{n\ell}\omega^2_{n\ell}\Gamma_{n\ell} \sum_{m,\omega} \sum_{\ell',m'} (L^{\ell'm'}_{\ell m})^2 [(\omega_{n\ell'm'} - \omega)^2 + (\Gamma_{n\ell'}/2)^2]^{-1}}. \tag{D14}$$

The numerator and denominator are summed over all m and ω in the m-dependent interval $\omega \in (\omega_{n\ell m} - 2\Gamma_{n\ell}, \omega_{n\ell m} - 2\Gamma_{n\ell})$. This provides an overall normalization constant to be applied at each radial order and harmonic degree. Note that because we only consider coupling at the same radial order, we drop the subscript n on the mode normalization constant N_ℓ.

E. SURFACE-TAIL CONSTRAINT

In the expression (33), we apply two penalties (λ and ν), the former to diminish sensitivity to undesired wavenumbers and the latter to the overall surface tail. Since modes spend a lot of
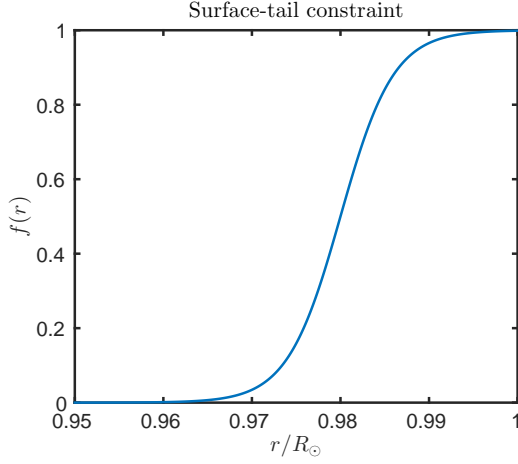
Figure 9. Surface-tail constraint function $f(r)$, as used in equation (33) and described in equation (E15). The function is zero for most of the interior and rises sharply in the outer 2.5% of the solar radius or so.

time near the surface layers, kernels typically tend to be dominantly sensitive to surface layers. Only when taking a coherent weighted sum of the kernels can the surface sensitivity be removed. However, in the present case, numerous wavenumbers contribute to the overall sensitivity. Weights designed for a specific (s, t) that result in sensitivity at depth, for instance, do not produce the same depth sensitivity in adjacent (s', t') wavenumbers (as in Figures 1 through 4). In fact, because the sum is not necessarily coherent in the same manner, the sensitivity of the adjacent wavenumbers is to the surface. We can therefore penalize sensitivity to the surface layers as an indirect means of mitigating leakage in the (s, t) space. Note that this doesn't apply when imaging the immediate sub-surface layers, and so we set $\nu = 0$ in that case, and choose finite λ instead in equation (33).

For the function $f(r)$, we choose the following

$$f(r) = \frac{1}{1 + \exp \frac{0.98 R_\odot - r}{0.003 R_\odot}},$$ (E15)

plotted in Figure 9.